SLAC-PUB-12474
April 17, 2007

Proposed laser-driven, dielectric microstructure few-cm long undulator for attosecond coherent X-rays

T. Plettner and R.L. Byer

E.L. Ginzton Laboratories, Stanford University, Stanford, CA 94305

This article presents the concept of an all-dielectric laser-driven undulator for the generation of coherent X-rays. The proposed laser-driven undulator is expected to produce internal deflection forces equivalent to a several-Tesla magnetic field acting on a speed-of-light particle. The key idea for this laser-driven undulator is its ability to provide phase synchronicity between the deflection force and the electron beam for a distance that is much greater than the laser wavelength. The potential advantage of this undulator is illustrated with a possible design example that assumes a small laser accelerator which delivers a 2 GeV, 1 pC, 1 kHz electron bunch train to a 10 cm long, ½ mm period laser-driven undulator. Such an undulator could produce coherent X-ray pulses with ~10^9 photons of 64 keV energy. The numerical modeling for the expected X-ray pulse shape was performed with GENESIS, which predicts X-ray pulse durations in the few-attosecond range. Possible applications for nonlinear electromagnetic effects from these X-ray pulses are briefly discussed.

PACS numbers: 41.60.Cr, 41.75.Jv, 41.75.Ht, 42.25. Bs

Submitted to Physical Review

Work supported in part by US Department of Energy contract DE-AC02-76SF00515

SLAC, Stanford University, Stanford, CA 94309

I. INTRODUCTION

Generation of ultra-short pulse radiation at ever-smaller wavelengths is rapidly gaining interest in many branches of the basic and applied sciences. Free Electron Lasers (FELs) that rely on Self-Amplified Spontaneous Emission (SASE) appear to be especially well-suited to this end. The concept of self-amplified spontaneous emission free-electron laser radiation (SASE-FEL) was first explored in 1984 [1]. The SASE-FEL is a single-pass process where the electron beam interacts with its very own produced undulator radiation field and under certain conditions amplifies the co propagating electromagnetic wave to saturation. This process does not require cavity mirrors or other optics and therefore is ideally suited to produce radiation at wavelengths for which low-loss optics are not possible to manufacture. SASE-FEL devices have been demonstrated in the near-infrared [2] and in the UV [3], and near future SASE-FEL facilities like the Linear-Coherent Light Source (LCLS) [4] or the X-Ray Free-Electron Laser (XFEL) [5] will produce coherent femtosecond time-scale X-rays at λ_r ~ 1Å wavelengths.

The ability of free electron lasers to produce short wavelengths lies in the Doppler shift of the electromagnetic radiation from the relativistic electrons traversing the undulator when observed from the laboratory frame. The center wavelength λ_r of FEL depends on the kinetic energy of the electron and on the undulator period λ_u, and for weak undulators is approximately given by $\lambda_r \sim \lambda_u / 2\gamma^2$, where γ is the time dilatation constant that is proportional to the kinetic energy for relativistic electrons. Typical conventional permanent magnet undulators have periods on the order of 1 cm or longer and hence require multi-GeV electron beams to reach the desired X-ray wavelengths.

Therefore, RF-accelerator driven X-ray FEL facilities will have a total length on the order of one kilometer.

Although the realization of an integrated all-laser-driven particle accelerator still lies in the future the possibility for employing such an accelerator for a SASE-FEL device is interesting to explore. A few-meter long laser accelerator is expected to provide a GeV energy electron beam into an undulator and due to optical bunching at near-infrared wavelengths the electron pulse structure could provide attosecond time-scale radiation. To take advantage of such an accelerator a matching compact high-strength undulator would be highly desirable. In this article we explore a possible laser-driven undulator structure that produces significantly larger deflection forces than those attainable with permanent magnets. The result is a predicted enhancement of the FEL growth rate that allows for very a short undulator.

II. THE PROPOSED LASER-DRIVEN SASE-FEL SYSTEM

In essence, a SASE-FEL system consists of three components: an electron injector that produces a train of free-electron bunches, a particle accelerator that boosts them to high kinetic energies, and an undulator that causes the bunches to produce electromagnetic radiation. We envision a SASE-FEL system that is entirely composed of dielectric based microstructures, from the electron injector to the undulator. Figure 1 illustrates the conceptual layout for an all-laser driven free electron radiation source. One of the main differences to conventional free-electron lasers is the use of a modelocked laser instead of a klystron to drive the electron beam. The modelocked laser source provides a higher

pulse repetition rate and a wavelength that is shorter by about 4 orders of magnitude, which is a key condition for the possibility of electron bunches with durations in the attosecond range. In spite of the relatively low electron bunch charges expected from laser particle accelerators the predicted attosecond electron pulse structure will allow for high peak currents that are required for an effective, short-undulator FEL.

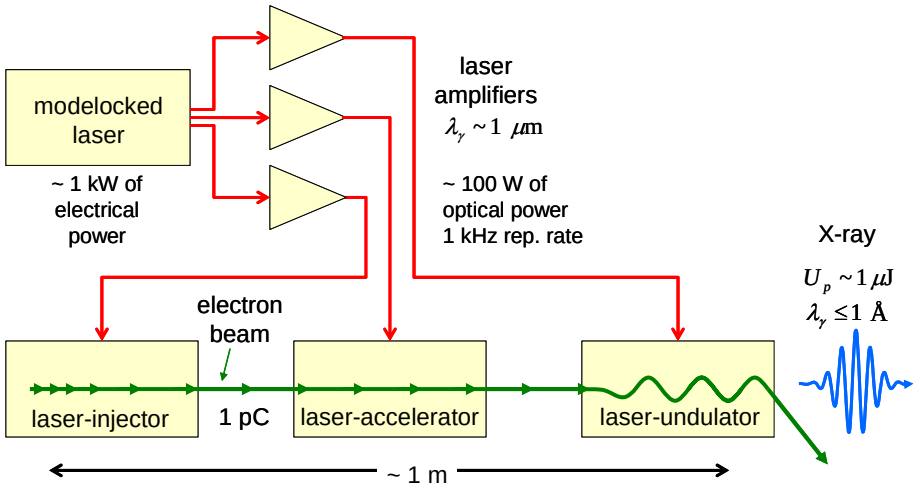

FIG. 1. Schematic of a possible tabletop laser-driven SASE-FEL system

A final characteristic of the proposed system is its potential for a moderate power requirement. Depending on the laser-accelerator geometry the coupling efficiency from the laser to the electron beam is on the order of ~5% [6]. Assuming a worst-case coupling efficiency estimate of one percent and a maximum bunch charge of 1 pC a kHz repetition rate GeV electron beam requires on the order of 100 W of optical power. This output optical power lies well within reach of existing tabletop ultra-stable laser oscillators followed by moderate laser amplification stages. Laser systems with a ten-percent

wallplug efficiency or better are commonplace, and therefore a kilo-Watt electrical power FEL system that relies on the proposed components is conceivable.

Extensive research on laser driven electron sources and dielectric laser-driven accelerators is being pursued for a number of different applications. Laser-driven field emission tips offer the possibility of an ultra-low emittance, high brightness free-electron source [7,8]. Present research of field emission cathodes in rf electron guns suggests the possibility for reaching 10^{-9} m-rad normalized emittance [9]. The potential of GeV/m acceleration gradients from dielectric laser-driven particle accelerators was realized early on [10] and subsequently different microstructure-based architectures have been investigated [11,12,13,14,15,16]. Although an integrated laser-driven microstructure accelerator does not exist at the present time the physical process of linear laser-driven particle acceleration in vacuum has been observed [17] and several different dielectric accelerator microstructure prototypes will be tested with a relativistic electron beam in the near future [14,18,19]. E. Colby and P. Musumeci [20] have prepared concise review on the recent progress and of the future challenges for structure-based laser-driven particle accelerators.

In this article we first describe the envisioned architecture of laser-driven particle deflection and how this principle can be employed to devise an effective undulator structure. Next we present a specific undulator design powered by a laser-driven particle accelerator beam with a set of desired electron beam parameters and estimate the expected output FEL X-ray pulse.

III. THE OPERATION PRINCIPLE OF THE LASER-DRIVEN UNDULATOR

The key aspect of the proposed laser-driven undulator is the maintenance of phase synchronicity between the electromagnetic field and the traveling particle, which is designed to extend for a distance that is much larger than the wavelength of the driving electromagnetic wave. Such a condition decouples the laser wavelength from the undulator period and hence allows for use of near-infrared, high peak power laser beams that drive undulators with arbitrarily long periods.

The extended synchronicity condition can be accomplished by introducing a periodic phase modulation of the electromagnetic wave near the particle trajectory. A plane electromagnetic wave is launched orthogonal to the particle beam and the periodic phase modulation is introduced by the near field structure. This concept for introducing extended phase-synchronicity has been explored for a resonating laser-accelerator structure [13] and subsequently for a non-resonant laser-accelerator structure [14]. The symmetry of these accelerator structures does not allow for a synchronous deflection force that can act on the particle beam over several structure periods. However, as described in Appendix A, a configuration where the periodic structure is oriented at an angle to the electron beam satisfies phase synchronicity with a non-zero deflection force acting on a speed-of-light particle. Figure 2 shows the configuration that includes the oblique orientation between the structure and the electron trajectory. It can be shown that in such a configuration the average deflection from the transverse electric field and the average deflection from the magnetic field component do not fully cancel each other.

When the structure is powered with an ultra-short pulse laser beam, the incident electromagnetic wave has to have a pulse front tilt angle ψ such that $\tan\psi = \csc\alpha$ to maintain extended phase synchronicity with the particle beam [21].

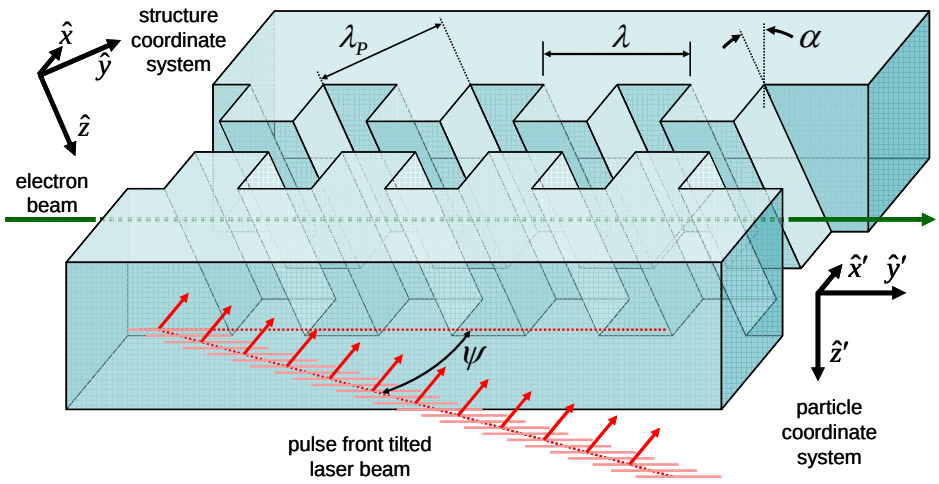

FIG. 2. Diagram of the proposed laser-driven deflection structure. The electron beam is propagating in the y' direction and the electromagnetic wave is polarized in the *yz* plane.

As shown in Figure 2, λ represents the center wavelength of the laser and λ_p is the period of the structure. At synchronicity the structure period and the laser center wavelength are related by $\lambda_p = \lambda\cos\alpha$. When this condition is satisfied we can define the average deflection gradient as

$$\left\langle \vec{G}_\perp \right\rangle = \left\langle \vec{F}_\perp / q(\vec{r},t) \right\rangle = \frac{1}{\lambda_p}\int_0^{\lambda_p} \vec{E}_\perp(\vec{r},t) + \left(\vec{v}\times\vec{B}(\vec{r},t)\right)_\perp dy \qquad (1)$$

where $\vec{E}$ and $\vec{B}$ are the electric and the magnetic from the laser sampled by the particle. As shown in equation 1 the deflection depends on both the transverse electric and magnetic field components.

To form an undulator from the laser-driven deflection structure a phase shift of π has to be added to the laser plane wave every M_u structure periods, such that the effective undulator period is $\lambda_u = 2M_u\lambda$. This type of condition reverses the direction of the deflection force once every M_u structure periods. Since the undulator period is much longer than the laser wavelength the π–phase shift can be introduced in the far-field by external optical elements, or it can also be included as part of the MEMs structure.

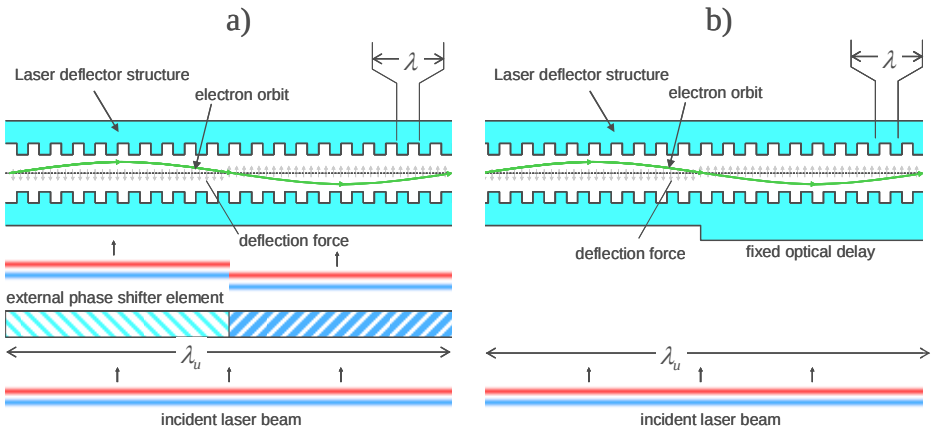

FIG. 3. Schematic of two possible external π-phase shift methods. (a) With an external optical phase shifter. (b) With a MEMs based fixed-distance delay element printed on the structure

Figures 3a and 3b show a schematic of the two possible phase shift schemes. Introduction of the phase shift by an optical element as shown in figure 3a in the far-field allows for flexibility in the choice of the undulator period length. For example, an electro-optic or even liquid-crystal device could allow for a programmable undulator period without having to replace the laser-driven deflector structure. The near-field permanent optical delay approach shown in Figure 3b may not have this flexibility but is more robust and may be better suited for high laser peak powers and the radiation environment. The most convenient approach will ultimately depend on the application in question. Topologically the proposed laser-driven undulator structure bears some resemblance to the permanent-magnet micro- wiggler structure [23] or to the grating based free electron laser concept [24,25]. The fundamental difference is that the functionality of the binary step surface of the vacuum channel is to provide phase synchronicity of the laser wave with the particle while the undulator period is provided by the external π-phase shifter. A variety of other micro-undulator schemes that rely on a completely different deflection mechanism than described here, such as magnetoresonance based [26], or crystalline based microunduators [27] have been investigated.

IV. A CRYSTAL QUARTZ BASED LASER-DRIVEN UNDULATOR

A specific structure example that delivers a significant deflection gradient is discussed in this section. Although crystal quartz may not be the ultimate material of choice for this application its nanofabrication technology is well developed and hence it is potentially an ideal test substrate for the conceptual ideas explored here. Quartz has an index of refraction of 1.58 at 800 nm. For simplicity we consider a geometry with a grating tilt

angle $\alpha = 20°$ and a grating duty cycle of ½ and a vacuum channel width of 0.4λ, as shown in Figure 4. Numerical evaluation of the fields inside the vacuum channel by FD-TD was employed to determine the deflection gradient with equation 1. For the given parameters the optimum pillar height that yields the maximum deflection gradient $\left\langle \vec{G}_{\perp,TE} \right\rangle \sim 0.15 E_{laser}$ was is $l \sim 0.6\lambda$.

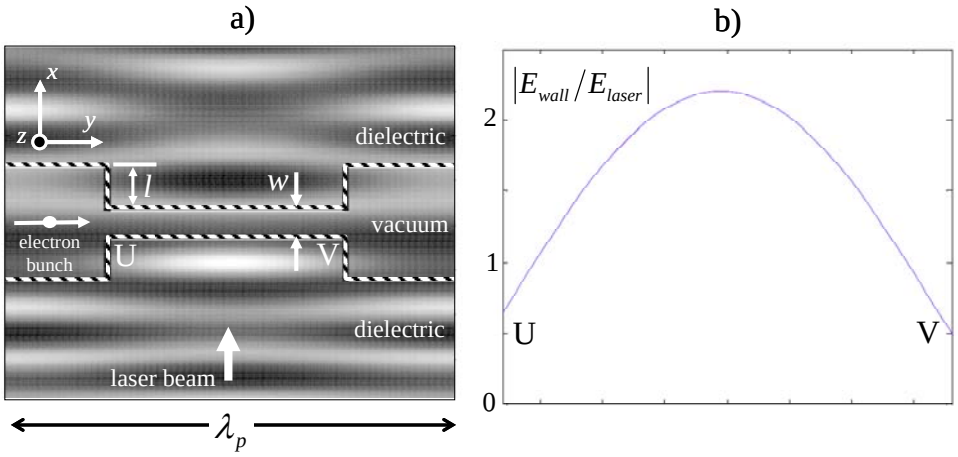

FIG. 4: a) map of $E_z(x, y)$ in one structure period produced by a TE wave. The pillar height l is 0.6λ while the vacuum channel width w is 0.4λ. The white arrow indicates the direction of the incident plane wave. b) the peak electric field amplitude at the structure surface at the narrow channel region between corner points U and V.

Figure 4a shows a grayscale map of $E_z(x, y)$ from a TE wave in one structure period at a particular instant, and Figure 4b shows the peak amplitude of E_z at the surface of the pillar at the narrow region of the vacuum channel between the corner points labeled U and V. The peak electric field is located at the center region of the pillar surface and is about twice the input laser amplitude; $|E_{\max}| \sim 2|E_{laser}|$. The field amplitude near the

corner points U,V is only about a third of $|E_{\max}|$. The lower optical field value near the corners is desirable since the laser breakdown threshold at a sharp edge is lower than that at the flat region. When expressed in terms of the local maximum surface field illustrated in Figure 4b, the average gradient for the TE mode is $\langle \vec{G}_{\perp,TE} \rangle \sim 0.07 |E_{\max}|$. The surface dielectric breakdown strength from ultra-short laser pulses with $\tau < 1$ psec has been observed to break the $\tau^{1/2}$ dependence seen with longer pulses and to remain near 1-2 J/cm^2 [28,29]. Hence the maximum peak electric field at this fluence from a 10 fsec laser pulse is approximately $|E_{\max}| \sim 25\,\mathrm{GV/m}$, which leads to a maximum deflection gradient $\langle G_{\perp,TE} \rangle \sim 2\,\mathrm{GV/m}$. Taking into account further effects like beam loading and structure imperfections a deflection gradient of $\langle G_{\perp} \rangle \sim 1\,\mathrm{GV/m}$ is a more realistic and conservative estimate. This deflection gradient corresponds to an equivalent magnetic deflection force of ~3T on a speed-of-light particle. With the expected deflection gradients it is very natural to consider replacing a permanent magnet based undulator with this type of laser-driven structure. Here the deflection strength is dependent on the optical phase, and a π-phase shift reverses the direction of the deflection.

V. THE EXPECTED FEL GAIN FROM THE LASER-DRIVEN UNDULATOR

The key parameters that determine the FEL amplitude growth rate of an undulator are its deflection strength and the electron peak density n_e. In a planar undulator carrying a magnetic field B_0 the steady-sate one-dimensional small-signal growth rate Λ for the electromagnetic wave intensity has the form [30]

$$I(z) = I_0 e^{\Lambda z}, \quad \Lambda \propto B_0^{2/3} n_e^{1/3} \tag{2}$$

The lower emittance and the attosecond pulse structure from a laser-driven particle accelerator are the two key expected traits that can lead to an enhanced peak electron density n_e and hence to a larger FEL gain. Since the structure-based laser-driven particle accelerators operate in the same fashion as RF linear accelerators they are expected to display a similar energy spread $\Delta\gamma/\gamma$ on the order of a fraction of one percent. Furthermore since the wavelength of the driving electromagnetic field is reduced by four orders of magnitude their electron bunch duration is expected to scale down to a few attoseconds. The transverse invariant emittance supported by structure based laser-particle accelerators has been predicted to be capable of reaching emittance values on the order of 10^{-9} m-rad or lower [13,31]. The bunch charge from laser-driven accelerators is estimated from beam loading considerations, and there is a wide range of expected bunch charge values that depends on the specific accelerator geometry. For example, photonic bandgap waveguide based accelerators have a very small vacuum channel area and are expected carry ~1fC per bunch [32] while proposed transverse laser-pumped planar accelerator structures have a larger area vacuum channel and can therefore could potentially carry close to one pC per bunch [14]. We begin the analysis with 1 pC per bunch and later study the effect of lower bunch charges on the expected X-ray generation. GENESIS [33] is employed to model the FEL growth from the electron beam produced by the laser-driven accelerator. For simplicity a round electron beam profile is assumed. The electron spot size and focusing were optimized for the most rapid FEL growth in the undulator. The optimum electron beam focusing parameters correspond to a

spot size of 180 nm and a focusing element every 50 undulator periods. The electron beam parameters desirable for a laser-driven FEL system and employed in GENESIS are summarized in Table I.

Assumed electron beam parameters	
Beam energy	2 GeV
Transverse emittance	10^{-9} m-rad [31]
Energy spread	0.5%
Bunch duration	5 attosec
Bunch charge	1 pC [14]
Spot size	180 nm

Table I: Theoretical electron beam parameters from a laser-accelerator

To illustrate the advantage of the proposed laser-driven undulator over a permanent magnet undulator we first consider an example where the 2 GeV electron beam with the parameters of Table I is directed into a conventional permanent magnet undulator with a maximum field $\langle B_0 \rangle \sim \frac{1}{2}\mathrm{T}$. We assume an undulator period of λ_u = ½ mm, which is unusually short for permanent magnet undulators and produces an undulator strength $K \sim 2.3\times10^{-2}$. However, as discussed later, the strong deflection force expected from a laser-driven undulator produces $K \sim 1.9\times10^{-1}$ and therefore allows for the consideration of sub-mm undulator periods. The combination of λ_u = ½ mm and a 2 GeV beam energy

result in a predicted SASE-FEL wavelength of $\lambda_r \sim$ 0.2 Å corresponding to a photon energy of ~64 keV.

Figure 5a shows the growth of the number of photons in the X-ray pulse versus the distance traveled by the electron beam inside the permanent magnet undulator. Figure 5b shows the corresponding time profile of the photon pulse at locations A,B,C and D inside the undulator. It can be appreciated that beyond ~1.0 m of undulator there is no sizeable increase in the photon number and that due to field slippage the pulse duration increases significantly. The passage of the electron beam through each undulator period introduces a time slippage between the electron and the FEL field of $\tau_r = \lambda_r / c$. For an undulator with N_u periods this adds up to a total time slippage $\tau_r = N_u \lambda_r / c$, and for 2000 undulator periods this corresponds to ~110 attoseconds. This accounts for the pulse duration shown for trace C and the further stretching observed of trace D.

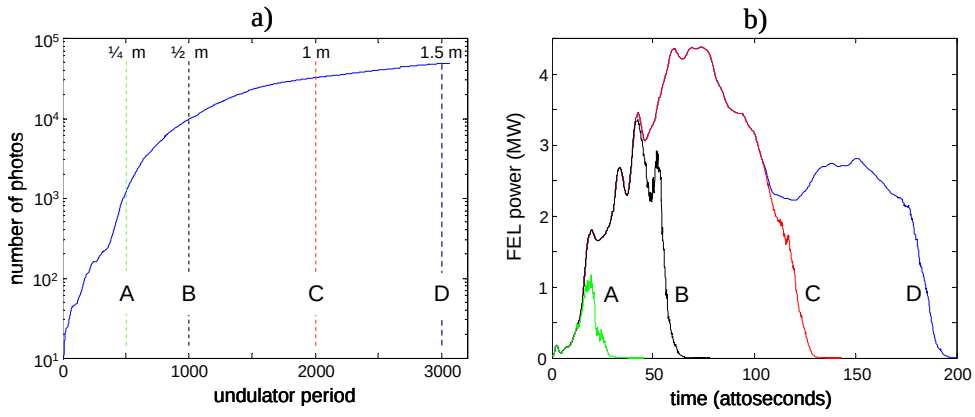

FIG. 5. (a) Growth of the photon field in a permanent magnet undulator of period λ_u = ½ mm and magnetic field $\langle B_0 \rangle$ = ½ T. (b) Time profile of the power of the X-ray pulse at locations A,B,C and D in the undulator.

The predicted X-ray traces in Figure 5b imply a very large undulator radiation component. Earlier reported work on the performance of such a permanent magnet undulator with laser-driven electron beam with one-dimensional simulations showed a significantly stronger FEL gain than that shown in Figure 5 [34]. Clearly the transverse emittance and the diffraction of the FEL field play a significant role in the degradation predicted be the three-dimensional model. As seen in Figure 5a, a maximum of only ~10^5 photons are produced by the bunch. Treating this photon number output as an effective saturation we estimate an FEL parameter $\rho_{eff} \sim N_{photon} \times E_{photon} / E_{kin} \sim 10^{-6}$, where E_{kin} is the total kinetic energy of the 1pC, 2 GeV electron bunch and E_{photon} is the energy of the individual X-ray photon. Therefore a permanent magnet micro-undulator is not effective to generate SASE-FEL from an electron beam with the parameters of Table I. Furthermore fabrication of such an undulator does not appear feasible. While individual ~1T surface field permanent magnets are commercially available, a few meters of such ½ mm long undulator periods correspond to thousands of such individual micro-magnets that would require separate alignment. To the author's knowledge there is no efficient permanent-magnet micro-fabrication technique for sub-mm domains with the desired peak field strength of ~1 T.

To contrast this shortcoming we analyze the performance of an equivalent laser-driven undulator powered by the same beam with parameters from Table I. A 1 GV/m deflection with λ_u = ½ mm corresponds to an undulator strength $K \sim 1.9 \times 10^{-1}$. Figure 6a shows the photon number of the X-ray pulse versus distance at optimum focusing parameters in a

laser-driven undulator and Figure 6b shows the corresponding predicted output photon pulse shape at locations A,B,C and D inside the undulator. For the laser-driven undulator the gain is so large that the pulse profiles in Figure 6b are shown on a logarithmic scale. Inspection of Figure 6a reveals that there is a clear exponential growth of the photon number having the form $N_{photon} \propto e^{\Lambda y} \equiv e^{y/L_G}$ where the gain length L_G is defined as the inverse of the growth rate Λ and is about 7 mm. This translates to an effective FEL parameter $\rho_{eff} = \lambda_u / \left(4\sqrt{3}\pi L_{G,eff}\right)$ of $\rho_{eff} \sim 3\times 10^{-3}$. This value for an FEL parameter predicts a total photon flux $N_{photon} = \rho_{eff} \times E_{kin} / E_{photon}$. The values of E_{kin} and E_{photon} are the same as in the previously analyzed case of the permanent magnet undulator and thus the FEL parameter predicts a photon saturation number $N_{photon} \sim 10^9$. Figure 6a shows agreement with this saturation number estimate. Finally, the FEL field mode size predicted from this FEL parameter value is $\sigma_{FEL} \sim \sqrt{\lambda_u \lambda_r / \rho_{eff}} \,/ 4\pi \sim 150\,\text{nm}$. This value is consistent with the electron spot size of 180 nm employed in the GENESIS simulation corresponding to the traces in Figure 6.

The saturation energy from 10^9 photons corresponds to 10 μJ of X-rays per electron bunch. Therefore a dielectric based laser-driven undulator appears to be feasible for the effective production of high peak power X-ray pulses. Furthermore the very short gain length allows for few-attosecond coherent X-ray pulses. However, one potential limitation of a laser-driven undulator is the very narrow vacuum channel that could lead to clipping of the diffracting FEL field and consequently to a reduction in gain. It

becomes therefore important to verify that the FEL growth rate outdoes the loss rate from clipping.

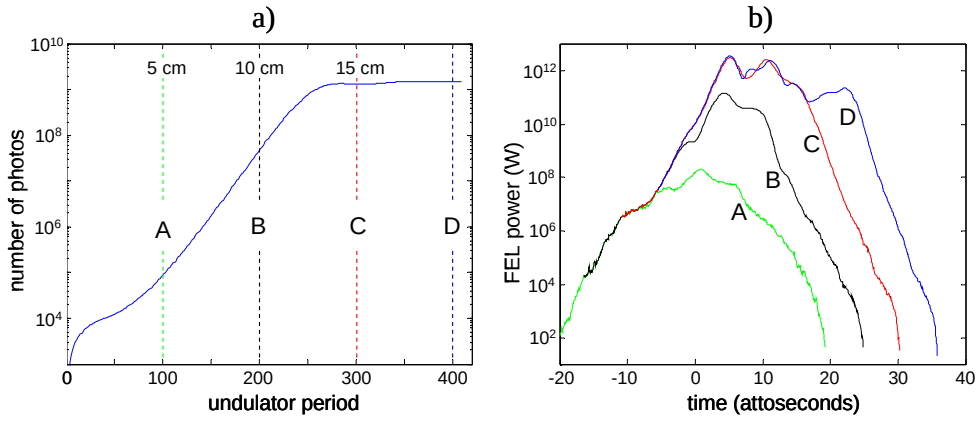

FIG. 6. (a) FEL amplitude growth in a laser-driven undulator of period λ_u = ½ m and deflection gradient $\langle G_\perp \rangle = 1\,\mathrm{GV/m}$, equivalent to a magnetic field $\langle B_0 \rangle$ = 3 T. (b) Evolution of the time profile of the FEL at points A,B,C and D inside the undulator.

Table II includes a set of parameters that allow for an estimate of the FEL field diffraction and also identify the expected FEL operation regime. The Rayleigh range of the FEL beam and divergence angle in Table II are estimated from the FEL wavelength and from the assumption of a Gaussian FEL field profile initially matched to the spot size of the electron beam at the input of the undulator. At the selected Ti:Sapphire laser wavelength of 0.8 μm the laser-driven undulator has an aperture of ~½ micron. With the divergence angle of the photon beam specified in Table II clipping of the wings of the FEL field begins to occur after 2 cm of propagation, which is much longer than the gain length. Hence the loss from clipping is not expected to play an important role. However

for the upcoming low-bunch charge examples analyzed in the next section the FEL gain length is much longer and loss of the FEL field from clipping may become an important factor to consider.

Parameter	**Value**
Optimum electron spot size	180 nm
Electron density	1.6×10^{23} cm^{-3}
Beam plasma frequency	3.6×10^{14} Hz
Photon Rayleigh range	5 mm
Photon beam divergence angle	30 μrad

Table II: Optimum electron beam and the corresponding optical field parameters

The modeled FEL processes in Figure 5 and 6 include space charge. To illustrate the effect of space charge Figure 7 shows the expected SASE FEL pulses in a laser driven undulator of period λ_u = ½ m and deflection gradient $\langle G_\perp \rangle = 1\,\mathrm{GV/m}$ with space charge turned off (trace A) and turned on (trace B). It can be observed that while there is degradation of the predicted FEL amplitude growth from space charge it is not severe, and that this shortcoming can be compensated with a slightly longer undulator. The few-attosecond pulse structure is not severely affected by space charge.

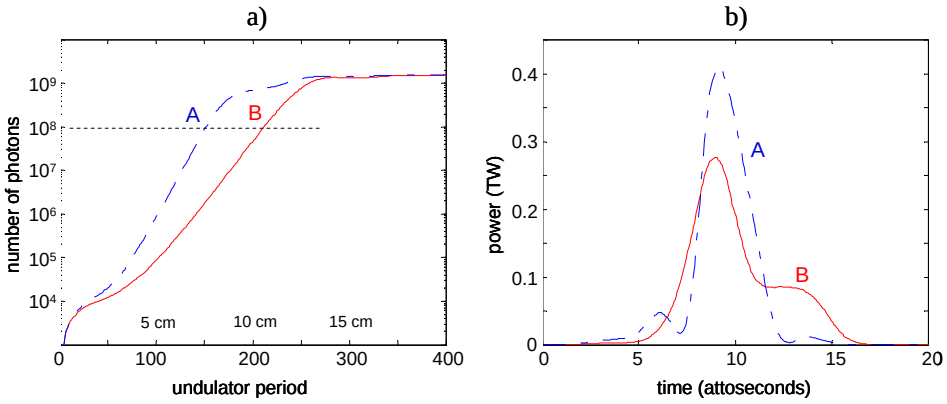

FIG. 7. (a) FEL amplitude growth for an electron bunch with parameters of table 1 in a laser-driven undulator. The solid line includes space charge while the dashed line does not. (b) FEL temporal pulse profiles for traces A and B at the undulator location where they generate 10^8 photons per pulse

The minimal effect of space charge predicted by GENESIS is in agreement with the chosen set of parameters belonging to the Compton regime. The condition for operation for this FEL operation regime [35] is satisfied when

$$\frac{\omega_p}{\gamma^{1/2} c k_u} << \frac{1}{16}\gamma_z^3 K^2 \tag{3}$$

where ω_p is the plasma frequency, $k_u = 2\pi/\lambda_u$, K is the undulator strength, and $\gamma_z \sim \gamma$ since for the laser-undulator $K \sim 0.19$. With the parameters of Tables I and II the left hand side of equation 3 is $\omega_p / c k_u \gamma^{1/2} \sim 1.5$ while the right hand side is

$\gamma^3 K^2/16 \sim 10^8$, confirming that with the given electron beam parameters space charge plays no major role. Furthermore, the electron beam plasma frequency listed in Table II is much smaller than the critical plasma frequency $\omega_c \sim \gamma^{3/2} K^2 c/\lambda_u \sim 10^{16}$ Hz.

VI. FEL GAIN FROM ULTRA-LOW BUNCH CHARGES

As stated earlier the optimum charge per bunch depends on the specific laser accelerator architecture, and for some proposed structures the estimated bunch charges are as low as 1 fC. With the wide range of possible bunch charges it becomes important to analyze the effect of bunch charge on the ability to produce X-rays from the proposed laser-driven undulator. Figure 8a shows the predicted FEL growth with the electron beam parameters of Table I and different bunch charges versus undulator length. As expected, both the FEL growth rate and the maximum number of photons suffer a dramatic decrease from the reduction of bunch charge.

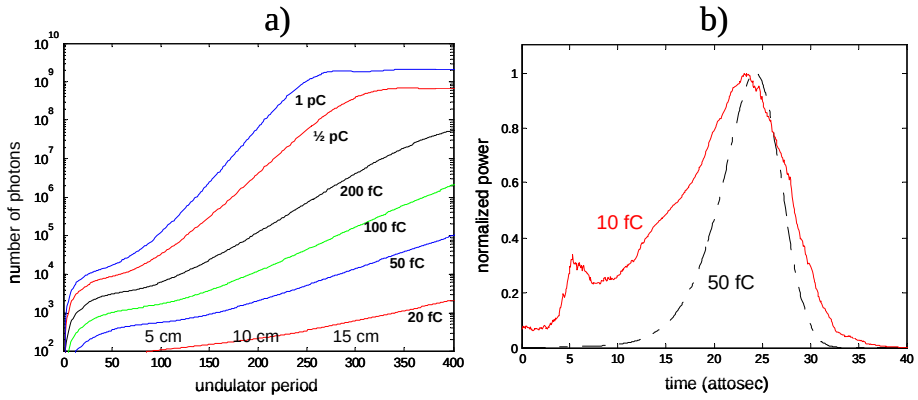

FIG 8: a) FEL pulse energy growth in a laser-driven undulator with a deflection gradient $\langle G_\perp \rangle \sim 1\,\mathrm{GV/m}$ for various electron bunch charges. b) Comparison of the temporal profile of the radiation between a 10 fC and a 50 fC electron bunch after 400 undulator periods.

For bunch charges below 20 fC the undulator radiation component becomes comparable or larger than the FEL amplification. Figure 8b illustrates this by comparing the pulse profiles for a 10 and a 50 fC electron bunch normalized to their peak values. The 50 fC bunch still shows a clear SASE-FEL pulse with exponential gain after 400 undulator periods while the X-ray output from a 10 fC bunch is reduced to mostly undulator radiation with only a very moderate amount of gain. With the given set of undulator parameters production of significant coherent FEL radiation from bunch charges below 10 fC does not appear feasible. Therefore, the development of a high bunch charge structure will be important if coherent X-ray generation with laser-driven particle accelerators is to become feasible.

VII. POSSIBLE APPLICATIONS

The very short expected X-ray pulse duration from the described laser-driven FEL system is expected to lead to very large peak electric fields and consequently to the possibility of nonlinear optical applications with moderate pulse energies. As shown in Figures 7b and 8a a 1 pC electron bunch charge is expected to produce X-rays with ~10^9 photons per FEL pulse with a duration below 10 attoseconds, corresponding to a peak power close to 1TW and to a peak electric field of ~10^{14} V/m. Depending on the produced photon energy the application of such field amplitudes on matter could lead to the study of nonlinear optical processes involving the core electrons such as proposed for coherent Raman spectroscopy [36]. Furthermore, the ultra short pulse durations potentially allows for unprecedented time resolution in pump-probe experiments such as those presently

carried out with soft X-rays from high-harmonic generation to study electron transfer dynamics [37].

The possible application of near-future conventional X-ray FEL facilities for electron-pair production and other nonlinear vacuum polarization and nuclear processes has been considered [38,39]. The adaptation of the low-power tabletop FEL design presented here to higher photon energies could lead to a unique high-energy physics machine that features relatively compact dimensions. Furthermore, the ability for the control of the polarization of the FEL pulse and the high repetition rate of the drive-laser offer a unique advantage for a photon-photon collider that could study nonlinear light-light vacuum reactions such as $\omega_1 + \omega_2 \rightarrow \omega_3 + \omega_4$, electron-positron pair production $n_1\omega_1 + n_2\omega_2 \rightarrow e^+e^-$, or potentially even higher-energy particle pair creation processes. The possibilities and limitations of a laser-driven FEL for this application will be explored more rigorously in an upcoming publication.

VIII. SUMMARY

The large deflection gradients from the proposed laser-driven undulator and the electron beam properties from a structure based laser-particle accelerator are the two essential aspects that could allow for an ultra-compact undulator and for the possibility of few-attosecond X-rays. The expected few-cm interaction length required from a laser-driven undulator implies that the entire undulator could be fabricated on a single quartz wafer, taking advantage of existing precision available nanofabrication technology. The possibility for an undulator as a single monolithic unit could present an important

advantage for addressing the tight alignment requirements and consequently could allow for a significant reduction of its fabrication cost.

The proposed concept was described in this article with a specific example, and the ultimate design will depend on the application in question. Possible improvements to the presented system include recycling of the laser beam that powers the accelerator structure [32], resonating of the X-ray photons [40] or recycling of the electron beam such as proposed for future X-ray FELs driven by superconducting accelerators [41]. Further possible improvements include the implementation of other substrate materials for the dielectric undulator and examination of shape factors other than a binary step function that was assumed in this article for vacuum channel.

The numerical modeling of the FEL process presented in this article constitutes a first order feasibility analysis of the concept, and more refined calculations will reveal the extent of the degradation of the FEL process from wakefield effects caused by the periodic rough surface of the structure of the vacuum channel [42] and by the undulator [43,44] and possible remedies such a tapering of the undulator field [42] or initial energy chirp of the electron beam [45]. Implementation of shorter-wave optical electron bunch compression techniques analogous to the combination of shorter-wavelength energy modulators and dispersive dogleg or chicane electron transport elements such as planed for the LCLS [4] , or as the proposed implementation optical bunchers to conventional electron beams from RF accelerators [46,47] could lead to further reduction of the X-ray FEL pulse that is already in the few-attosecond timescale without significant

complication to the system. This possibility is very appealing and will merit closer inspection. Finally, the driven FEL system such as the one described here may present a unique opportunity for efficient FEL harmonic generation. Depending on the polarization and optical phase of the drive-laser beam the laser-driven undulator structure can also provide a longitudinal force component with the same undulator period. This allows for an external control of the enhancement or mitigation of the figure-8 particle orbit responsible for FEL harmonics.

In summary, as future experimental work laser-driven particle accelerators evolves and as their advantages and limitations are revealed more detailed and realistic designs for a laser-driven FEL system that contain some of the mentioned capabilities such as recycling or bunch compression schemes or the possibility of harmonics will become possible. It can be concluded that, if successful, a laser-driven undulator presents a series of unique new possibilities for efficient generation of coherent X-ray radiation.

ACKNOWLEDGEMENTS

The authors would like to thank P. Hommelhoff for his advice on the capabilities and limitations from laser-driven field emission tips and their possible application to particle accelerators. Furthermore we thank R. Rice and H. Injeyan for their advice on possible future improvements to the proposed system and potential applications of an integrated laser-driven FEL device. We also thank R. Ischebeck and Z. Huang for valuable advice on SASE FELs. Finally, we greatly appreciate the support from Northrop Grumman for funding of this work.

APPENDIX A

The present analysis derives the phase synchronicity for a deflection force from a cw plane wave powering a two-dimensional periodic structure such as that shown in Figure 2. The particle is assumed to have a uniform, time-independent velocity $v \sim c$ and the structure is approximated by assuming infinite extent in the *z*-direction. This two-dimensional geometry supports two independent field solutions representing transverse-electric (TE) or transverse-magnetic (TM) waves. Both solutions have only three inter-dependent field components. For a TM wave the nonzero field components are E_x, E_y, and B_z. In the coordinate system of the structure the particle's velocity is $\vec{v} = c\left(\cos\alpha\hat{y} + \sin\alpha\hat{z}\right)$. Hence, in this coordinate system the Lorentz force from the TM wave acting on the relativistic particle is described by

$$\vec{F} = q\,\mathrm{Re}\begin{pmatrix} E_x + cB_z\cos\alpha \\ E_y \\ 0 \end{pmatrix} \tag{A.1}$$

As seen next, the $\cos\alpha$ term, which describes the oblique orientation between the structure and the particle orbit, is key for allowing a phase-synchronous deflection. The average gradients are defined as $\langle G_x \rangle_{\mathrm{TM}} = \langle F_x/q \rangle$, $\langle G_y \rangle_{\mathrm{TM}} = \langle F_y/q \rangle$, and $\langle G_z \rangle_{\mathrm{TM}} = \langle F_z/q \rangle$ evaluated along the particle path $y' = y/\cos\alpha$. Because of the periodicity of the structure and the normal incidence of the plane wave the field components have the form

$$E_x(0,y,t)=\sum_{n=-\infty}^{+\infty}U_n e^{ik_p ny}e^{ikct}$$
$$E_y(0,y,t)=\sum_{n=-\infty}^{+\infty}V_n e^{ik_p ny}e^{ikct} \qquad \text{(A.2)}$$
$$B_z(0,y,t)=\sum_{n=-\infty}^{+\infty}W_n e^{ik_p ny}e^{ikct}$$

where $k_p=2\pi/\lambda_p$ and $k=2\pi/\lambda$. In the vacuum channel the time harmonic fields E_x and B_z can be shown to be related by $cd_yB_z=ikE_x$. Therefore the coefficients of E_x and B_z are related by

$$cW_n=\frac{k}{nk_p}U_n \qquad \text{(A.3)}$$

The particle position in the vacuum channel is $y(t)=y_0+ct$. Therefore the time variable can be expressed as $t(y)=y/c-y_0/c$. Hence the average deflection gradient $\langle G_x\rangle_{\mathrm{TM}}$ can be described in terms of the Fourier coefficients

$$\langle G_x\rangle_{\mathrm{TM}}=\mathrm{Re}\left(e^{-iky_0}\sum_{n=-\infty}^{+\infty}\left[\left\{1+\frac{k\cos\alpha}{nk_p}\right\}U_n\lim_{L\to\infty}\left(\frac{1}{L}\int_0^L e^{i\left(k_p n+k/\cos\alpha\right)y'(y)}dy'\right)\right]\right) \qquad \text{(A.4)}$$

The term e^{-iky_0} is a constant that represents the optical phase of the particle with respect to the field and can be taken out of the path integral. For $\langle G_x \rangle_{\mathrm{TM}}$ to be nonzero there has to be a component in the sum of equation A.4 that possesses a non-oscillatory term, that is,

$$nk_p + k/\cos\alpha = 0 \tag{A.6}$$

When this condition is satisfied for the n$^{\mathrm{th}}$ coefficient in equation A.4 the average deflection gradient simplifies to

$$\langle G_x \rangle_{\mathrm{TM}} = \mathrm{Re}\left(e^{-iky_0} U_n\right) \sin^2\alpha \tag{A.7}$$

Equation A.7 establishes that a continuous, phase-synchronous deflection force can be produced by a TM polarized plane wave incident on a periodic structure. Notice that when the tilt angle α between the particle trajectory and the structure is zero no phase-synchronous deflection force is possible. Hence the necessity for a nonzero tilt angle and a structure geometry as shown in Figure 2. A similar condition is found to apply with the TE polarization.

This type of analysis can also be applied for oblique incidence plane waves and pulse-front tilted laser beams. For such laser beams it can be shown that in addition to equation A.6 a pulse-front tilt angle $\tan\psi = 1/\cos\alpha$ is required for phase synchronicity. Finally, it can also be shown that at phase-synchronicity the average deflection gradient can be

evaluated from the fields within one structure period as indicated in equation 1. A rigorous analysis that includes these aspects is presented elsewhere [21].

References

1. R. Bonifacio, C. Pellegrini, L.M. Narducci, "Collective Instabilities and high-gain regime in a free electron laser", Opt. Comm. 50, 373-378 (1984)
2. M. Hogan et al, "Measurements of Gain Larger than 105 at 12 μm in a Self-Amplified Spontaneous-Emission Free-Electron Laser", Phys. Rev. Lett. 81, 4867–4870 (1998)
3. J. Andruskov et al, "First Observation of Self-Amplified Spontaneous Emission in a Free-Electron Laser at 109 nm Wavelength", Phys. Rev. Lett. 85, 3825–3829 (2000)
4. SLAC-R-593, "Linac Coherent Light Source (LCLS) Conceptual Design Report", http://www.slac.stanford.edu/pubs/slacreports/slac-r-593.html (2002)
5. TESLA-FEL-2002-09 "Tesla XFEL Technical Design Supplement Report" (2002)
6. L. Schächter et al "Scaling Laws of a Dielectric Optical Accelerator" Proceedings of the 2003 Particle accelerator conference p. 722 (2003)
7. P. Hommelhoff, Y. Sortais, A. Aghajani-Talesh, M. A. Kasevich, "Field Emission Tip as a Nanometer Source of Free Electron Femtosecond Pulses", PRL 96, 077401 (2006)

8. P. Hommelhoff, C. Kealhofer, M. A. Kasevich, “Ultrafast Electron Pulses from a Tungsten Tip Triggered by Low-Power Femtosecond Laser Pulses”, PRL 97, 247402 (2006)
9. J.W. Lewellen, J. Noonan, “Field-emission cathode gating for rf electron guns”, Phys. Rev. ST AB 8 033502 (2005)
10. Y.C. Huang, D. Zheng, W.M. Tulloch, R.L. Byer, “Proposed structure for a crossed-laser beam GeV per meter gradient, vacuum electron linear accelerator”, Appl. Phys. Lett. 68, 753-755 (1996)
11. X. Eddie Lin, “Photonic band gap fiber accelerator”, Phys. Rev. ST AB, 4, 051301 (2001)
12. B. Cowan, “Two-dimensional photonic crystal accelerator structures” Phys. Rev. ST AB 6, 101301 (2003)
13. J. Rosenzweig, A. Murokh, C. Pellegrini, “A proposed dielectric-loaded resonant laser accelerator”, Phys. Rev. Lett. 74, 002467 (1995)
14. T. Plettner, P.P. Lu, R.L. Byer, “Proposed few-optical cycle laser–driven particle accelerator structure”, Phys. Rev. ST AB 9, 111301 (2006)
15. Z. Zhang, S. G. Tantawi, R. D. Ruth, “Distributed grating-assisted coupler for optical all-dielectric electron accelerator”, Phys. Rev. ST AB 8, 071302 (2005)
16. B. Cowan, “Three-Dimensional Photonic Crystal Laser-Driven Accelerator Structures”, SLAC-PUB-12090 (2006)
17. T. Plettner, R.L. Byer, E. Colby, B. Cowan, C.M.S. Sears, J. E. Spencer, R.H. Siemann, “Visible-laser acceleration of relativistic electrons in a semi-infinite vacuum”, Phys. Rev. Lett. 95, 134801 (2005)

18. T. Plettner, et al, “Structure Loaded Vacuum Laser-Driven Particle Acceleration Experiments at SLAC” , AIP Conference Proceedings 887, p. 103 (2006)
19. M. Lincoln et al, “Experimental Work with Photonic Bandgap Fiber: Building a Laser Electron Accelerator”, AIP Conference Proceedings 859, p. 103 (2006)
20. E. Colby, P. Musumeci, “Report of the Electromagnetic-Structure Based Accelerator Concepts Working Group”, AIP Conference Proceedings 183, p. 103 (2006)
21. T. Plettner, “Phase synchronicity conditions from pulse-front tilted laser beams in periodic structures”, SLAC-PUB-12458 (2007)
22. S.M. Rao, “Time domain electromagnetics”, San Diego : Academic Press, (1999)
23. G. Raiman et al, Nucl. Instrum. Methods, A 250, p. 125 (1986)
24. H.L. Andrews, J.E. Walsh, J.H. Brownell, “Designing a grating based free electron laser”, Nucl. Instrum. Methods, A 483, p. 478 (2002)
25. Y. Yao, Y.C. Huang, “Mode and gain analysis for symmetric and staggered grating-waveguide free-electron laser”, Phys. Rev. ST AB 10 030701 (2007)
26. G. Spindler, ; G. Renz, “Free-electron lasers:Scaling laws for microundulator operation in magnetoresonance with a strong guide field”, Physics of Plasmas 1, 398-403 (1994)
27. N. A. Korkhmazyan, N. N. Korkhmazyan, N. E. Babadganyan, “Crystalline Microundulator”, Technical Physics 49 499 (2004)
28. Y. Min Oh, S. Hyuk Lee, S. Park c, J. Sik Lee, “A numerical study on ultra-short pulse laser-induced damage on dielectrics using the Fokker–Planck equation”, International Journal of Heat and Mass Transfer 49 (2006) 1493–1500

29. B. C. Stuart et al, "Laser-Induced Damage in Dielectrics with Nanosecond to Subpicosecond Pulses", Physical Review Letters 74, 2248 (1995)
30. R. Ischebeck, PhD dissertation Thesis, “Transverse Coherence of a VUV Free Electron Laser”, DESY-THESIS-2003-033
31. B. Cowan, “Photonic Crystal Laser-Driven Accelerator Structures” PhD thesis, ch 3.5 particle beam dynamics (2007)
32. N. Na, R. H. Siemann, R. L. Byer, “Energy efficiency of an intracavity coupled, laser-driven linear accelerator pumped by an external laser”, Phys. Rev. ST AB 8, 031301 (2005)
33. S. Reiche, “GENESIS 1.3, a fully 3D time-dependent FEL simulation code”, Nucl. Instrum. Methods Phys. Res. A 429 243-248 (1999)
34. T. Plettner, R.L. Byer, “A proposed tabletop attoseconds pulse coherent X-ray source” Ultra-fast Phenomena conference proceedings, Pacific Grove, CA (2006)
35. H.P. Freund, T.M. Antonsen, “Principles of Free-electron Lasers”, Second edition, Chapman&Hall 1996
36. S. Tanaka, S. Mukamel, “Coherent X-ray Raman Spectroscopy: A Nonlinear Local Probe for Electronic Excitations”, Phys. Rev. Lett. 89, 043001 (2002)
37. A. Föhlisch et al, “Direct observation of electron dynamics in the attosecond domain”, Nature 436, p. 373-376 (2005)
38. T. J. Bürnevich, J. Evers, C. Keitel, “Nuclear Quantum Optics with X-ray Laser Pulses”, Phys. Rev. Lett. 69 142501 (2006)
39. S. P. Kim, D. N. Page, “Improved approximations for fermion pair production in inhomogeneous electric fields”, Phys. Rev. D 75 045013 (2005)

40. Z. Huang, R. Ruth, “Fully Coherent X-Ray Pulses from a Regenerative-Amplifier Free-Electron Laser”, Phys. Rev. Lett. 96, 144801 (2006)
41. J. Sekutowicz et al, “Proposed Continuous wave energy recovery operation of an X-ray free electron laser”, Phys. Rev. ST AB 8, 010701 (2005)
42. A. Mostacii, “Wakefields due to surface waves in a beam pipe with a periodic rough surface”, Phys. Rev. ST AB. 5 044401 (2002)
43. Z. Huang, K. Kim, “Review of X-ray free-electron laser theory”, Phys. Rev. ST AB 10, 034801 (2007)
44. S. Reiche et al, “Optimization of the LCLS X-ray FEL output performance in the presence of strong undulator wakefields”, SLAC-PUB-11773 (2005)
45. E. L. Saldin, E.A. Schneidmiller, M.V. Yurkov, “Influence of an energy chirp on SASE FEL operation”, Proceedings of the 27th International Free Electron Conference p. 258 (2005)
46. A.A. Zholents, W.M. Fawley, “Proposal for intense attosecond radiation from an X-ray Free-Electron Laser”, Phys. Rev. Lett. 92 224801 (2004)
47. A.A. Zholents, G. Penn, “Obtaining attosecond x-ray pulses using a self-amplified spontaneous emission free-electron laser” Phys. Rev. ST AB 8 050704 (2005)